Supporting information for

Noble-Metal Free, Atomically Thin $CuInP_2N_x$ Nanosheets for Highly Efficient, Stable, and Low-Cost Electrocatalysts in Acid Oxygen Evolution Reactions

Wentao Hou,[a] Xin Zhou,[b,c,*] Tingting Cheng,[a] Haoqiang Chi,[a] Yongcai Zhang,[d] Chen Zhuang,[a] Yubin Zheng,[a] Xiaohui Zhong,[e,*] Zhigang Zou,[a,f] and Yong Zhou[a, f, *]

[a] *School of Physics, Jiangsu Key Laboratory of Nanotechnology, Eco-materials and Renewable Energy Research Center (ERERC), National Laboratory of Solid-State Microstructures, Collaborative Innovation Center of Advanced Microstructures, Nanjing University, Nanjing, Jiangsu, 210093, P. R. China*

[b] *Interdisciplinary Research Center for Biology and Chemistry, Liaoning Normal University, Dalian, Liaoning, 116029, P. R. China*

[c] *College of Environment and Chemical Engineering, Dalian University, Dalian, Liaoning, 116622, P. R. China.*

[d] *School of Chemistry and Chemical Engineering, Yangzhou University, Yangzhou, Jiangsu, 225009, P. R. China*

[e] *School of Chemical and Environmental Engineering, Anhui Polytechnic University, Wuhu, Anhui, 241000, P. R. China.*

[f] *School of Science and Engineering, The Chinese University of Hong Kong (Shenzhen), Shenzhen, Guangdong, 518172, P. R. China;*

E-mail: zhouyong1999@nju.edu.cn; zhouxin@dlu.edu.cn; zxhui@ahpu.edu.cn

Contents

1.Materials

Powders of Cu, In, P and S element were purchased from *Shanghai Aladdin Biochemical Technology Co., Ltd*. All chemicals are of analytical purity and used as received without any pre-treatment.

2.Sample preparation

Preparation of $CuInP_2S_6$ crystals. Bulk $CuInP_2S_6$ crystals were prepared by solid-state sintering of corresponding metal elements in a quartz ampoule using a muffle furnace. Powders of Cu, In, P and S element were mixed with stoichiometric ratio (Cu : In : P : S=1 : 1 : 2 : 6 in molar ratio, about 1.2 g in total mass) and sealed into a quartz ampoule (18 cm in length and 12 mm in external diameter) under pressure of 1×10^{-4} torr. The ampoule was kept at 650 ℃ in the furnace for 5 days and naturally cooled down to room temperature. Finally, yellow $CuInP_2S_6$ crystals were collected inside the ampoule and grounded to powders.

Preparation of few-layer $CuInP_2S_6$ nanosheets. Few-layer $CuInP_2S_6$ nanosheets were prepared through sonication-assisted liquid phase exfoliation. The as-prepared

$CuInP_2S_6$ crystals were dispersed in 80 mL of ethanol and ultrasonicated for 2 days using an 1800 W cell crusher. Low-speed centrifugation was firstly conducted (3000 rpm, 6 minutes) to remove the insufficiently exfoliated bulks. The supernatant was decanted and further centrifuged at 12000 rpm for another 40 min to obtain few-layer $CuInP_2S_6$ nanosheets.

Preparation of $CuInP_2N_x$ nanosheets. $CuInP_2N_x$ nanosheets were prepared through ammoniation treatment in a tube furnace. Few-layer $CuInP_2S_6$ nanosheets were placed in a porcelain boat under ammonia (NH_3) flow (80 SCCM) and kept at certain temperature (200 ℃, 300 ℃, 400 ℃ and 500 ℃) for 5 h. The heating and cooling rate was set as 1 ℃ min^{-1}. Powders of $CuInP_2N_x$ were collected after the ammoniation treatment and noted as $CuInP_2N_x$-200, $CuInP_2N_x$-300, $CuInP_2N_x$-400 and $CuInP_2N_x$-500, respectively.

3.Characterization

The crystalline structure of samples was examined using a powder X-ray diffractometer (XRD, Rigaku Ultima III) with Cu-Kα irradiation (λ=1.5406 Å). Microscopic morphology of samples was investigated using a scanning electron microscope (SEM, Zeiss Gemini 500) coupled with energy-dispersive X-ray spectroscopy (EDX, Oxford Instruments Ultim Extreme) and transmission electron microscope (TEM, FEI Tecnai G2 F20S-TWIN). Chemical composition and states were measured using an X-ray photoelectron spectrometer (XPS, ULVAC-PHI PHI5000 VersaProbe). Electrochemical tests were carried out on an CHI660E electrochemical workstation (Shanghai Chenhua).

4.Electrochemical Measurements

Electrochemical measurements of samples were carried out in a conventional three-electrode configuration using 0.5 M H_2SO_4 solution as electrolyte (pH=0). A graphite rod electrode and a saturated calomel electrode (SCE) were chosen as counter

electrode and reference electrode, respectively. 2 mg of samples, 16 μL of Nafion solution (5 wt%), 100 μL of 2-Propanol and 384 μL of DI water were mixed by ultrasonication for 1 h to prepare catalyst inks. Then 16 μL of ink was uniformly drop-coated on a rotating disk electrode (RDE) and dried under room temperature to make working electrode. The diameter of glassy carbon disk on RDE is 5 mm (0.196 cm^{-2} in area). The measured potentials were calibrated to reversible hydrogen electrode (RHE) according to following formula:[1]

$$E_{(vs.\ \mathrm{RHE})} = E_{(vs.\ \mathrm{SCE})} + 0.244\ \mathrm{V} + 0.0591 \times \mathrm{pH} \quad (1)$$

An 90% *iR*-compensation was applied in LSV measurements to neutralize the ohmic potential drop when evaluating the OER performance. Electrochemical impedance spectra (EIS) were measured at open circuit potential with frequency ranging from 0.1 Hz to 10^5 Hz.

The electrochemically active surface area (ECSA) for electrocatalysts is estimated from the electrochemical double-layer capacitance (C_{dl}), which is extracted from cyclic voltammetry (CV) measurements conducted in a non-Faradaic region at different scan rates. Capacitive current density (*j*) was obtained according to the following formula:

$$j = \left| j_{\mathrm{charge}} - j_{\mathrm{discharge}} \right| / 2 = v C_{\mathrm{dl}} \quad (2)$$

where *v* is the scan rate. The slope of the linear fitting of *j* versus *v* gives the value of C_{dl}. The ECSA was further calculated using:

$$ECSA = \frac{C_{\mathrm{dl}}}{C_{\mathrm{s}}}$$

where C_S is the specific capacitance per unit area under identical electrolyte conditions. A typical value of C_S = 40 μF cm^{-2} under acidic conditions is adopted based on previous reports.

5.Computational Details

Density functional theory (DFT) calculations were conducted using the Vienna ab initio simulation package (VASP).[2, 3] The projector-augmented wave (PAW) method was applied to consider electron-ion interactions.[4] The Perdew-Burke-Ernzerhof (PBE)

functional within the generalized gradient approximation (GGA) was adopted for describing the exchange correlation.[5] A plane-wave cutoff energy of 450 eV was employed for the structural optimization and property calculations. The Brillouin zone integration was performed using a 7×3×3 Monkhorst-Pack type *k*-point mesh. Crystalline structure of bulk $CuInP_2S_6$ was constructed based on experimental data, and initial structure of $CuInP_2N_x$ was derived through substituting S atoms with N atoms in the parent $CuInP_2S_6$. The (001) surfaces of $CuInP_2S_6$ and $CuInP_2N_x$ were created by cleaving the relaxed bulk structure through the corresponding planes. A vacuum region of 15 Å was added along the *z*-direction to avoid mirror interaction between adjacent supercells. A Monkhorst-Pack *k*-point mesh of 5×3×2 is applied on structural and energetic calculations of both surfaces. Van der Waals correction was considered by utilizing DFT-D3 approach of Grimme.[6] Convergence thresholds of 10^{-5} eV for the energy and 0.01 eV $Å^{-1}$ for the forces were used for all optimizations. Since the PBE functional usually underestimates the band gap of semiconductors, a more accurate screened Coulomb hybrid functional HSE06 was adopted for calculating density of states.[7, 8] The mixing parameter α in HSE06 was set as the default value of 0.25 in this work.

The four-electron transfer involved OER process during water oxidation presents greater mechanistic complexity compared to the two-electron transfer HER process. To analyze the OER thermodynamics, the established framework developed by Nørskov and co-workers were employed by describing OER process through four consecutive proton-coupled electron transfer steps.[9, 10] Under standard conditions (pH=0, p=1 bar and T=298 K) using the standard hydrogen electrode as reference, the chemical potential of ($H^+ + e^-$) is equivalent to half the Gibbs free energy of H_2 formation. The thermodynamic driving force for each elementary step can be expressed through the following equation:[11]

$$\Delta G = \Delta E + \Delta ZPE - T\Delta S - eU \quad (3)$$

where ΔE is the energy change for each OER step, the zero-point energy change (ΔZPE) and entropic contributions ($T\Delta S$) are derived from calculated vibrational

frequencies and standard thermodynamics tables for gas-phase species. For adsorbed intermediates, the entropy is assumed to be negligible. The term of eU accounts for the applied electrochemical bias U in each proton-coupled electron transfer step. The overall free-energy change for the reaction $2H_2O \rightarrow O_2 + 2H_2$ is fixed at the experimental value of 4.92 eV. In an ideal OER catalyst, each intermediate step would have ΔG of 1.23 eV. However, real catalysts exhibit non-ideal energetics due to binding limitations. The OER overpotential (η^{OER}) is determined by comparing the most endergonic step to the ideal 1.23 eV benchmark, being expressed by the following equation:

$$\eta^{OER} = \frac{\Delta G_{max} - 1.23}{e} \tag{4}$$

where ΔG_{max} is the largest ΔG among the four elementary steps. The value of η^{OER} serves as a key descriptor of OER efficiency. A lower η^{OER} indicates that the potential-determining step requires smaller additional energy beyond the ideal 1.23 eV, implying more favorable reaction kinetics.

6.Figures

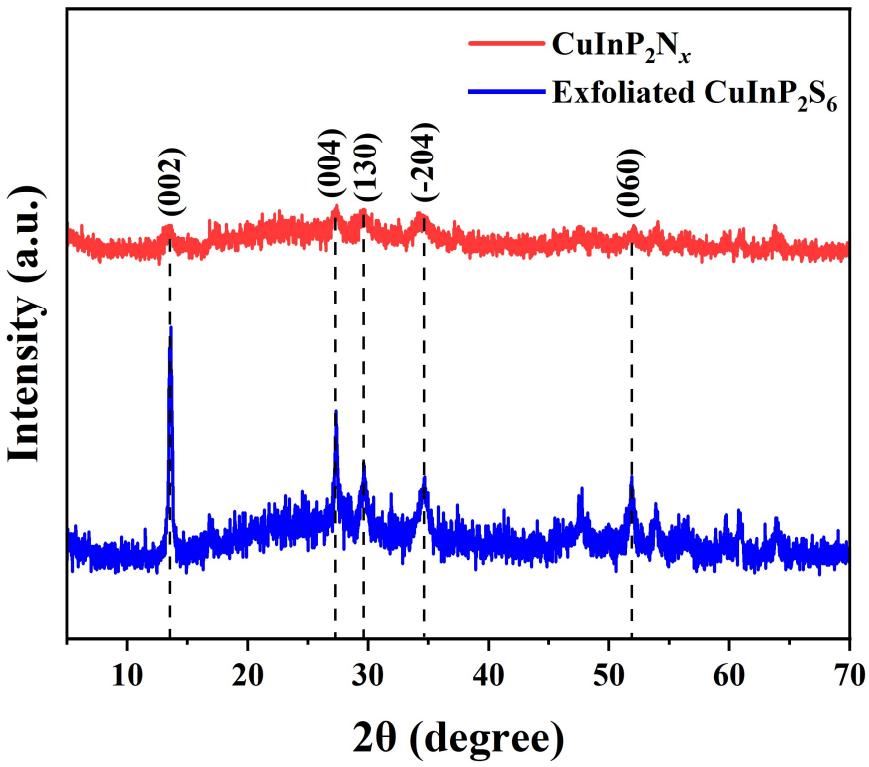

Fig. S1. XRD patterns of $CuInP_2S_6$ nanosheets and $CuInP_2N_x$-300.

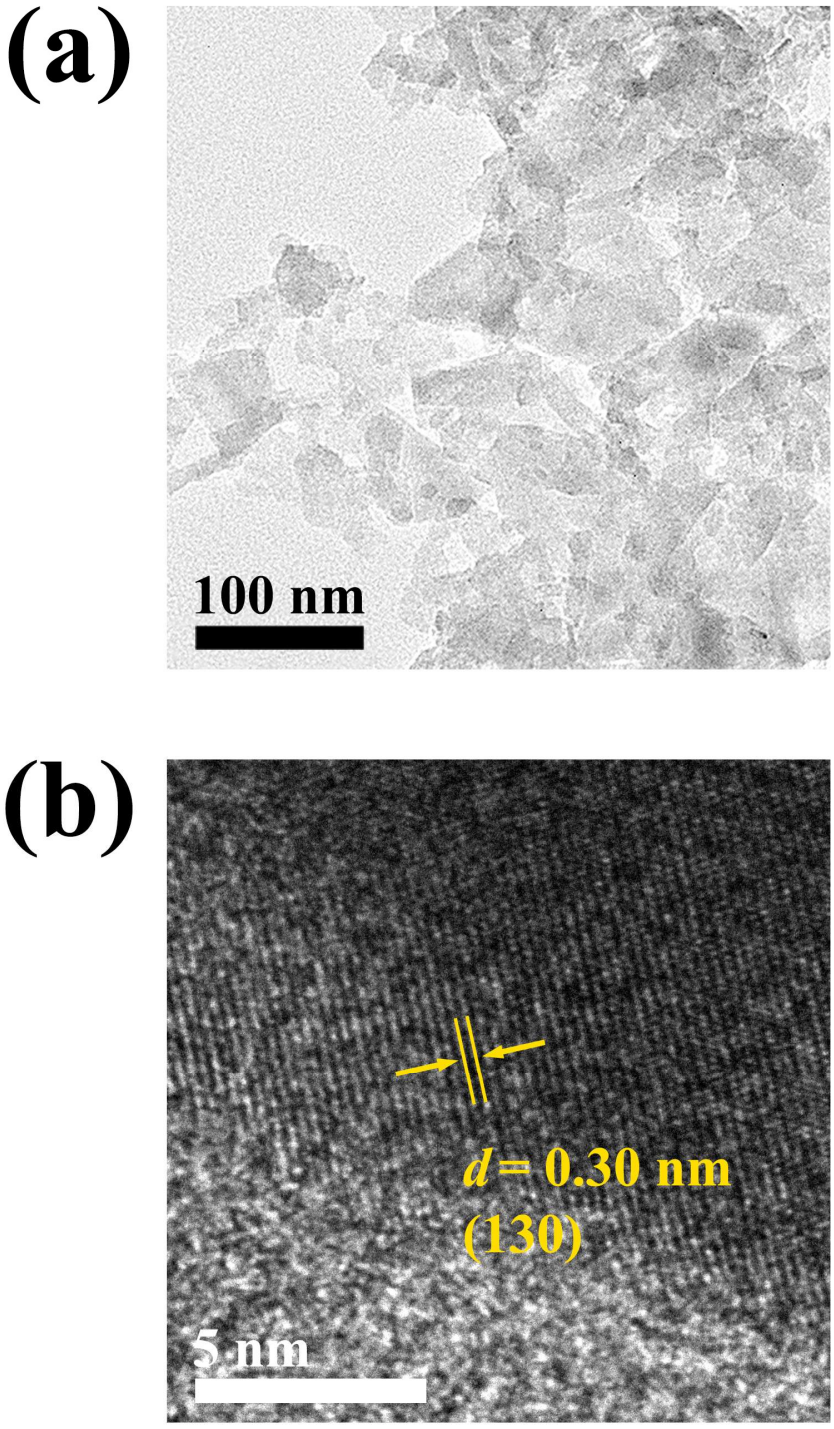

Fig. S2. TEM images of few-layer $CuInP_2S_6$ nanosheets.

Fig. S3. Photograph showing Tyndall effect in the ethanol dispersion of few-layer $CuInP_2S_6$.

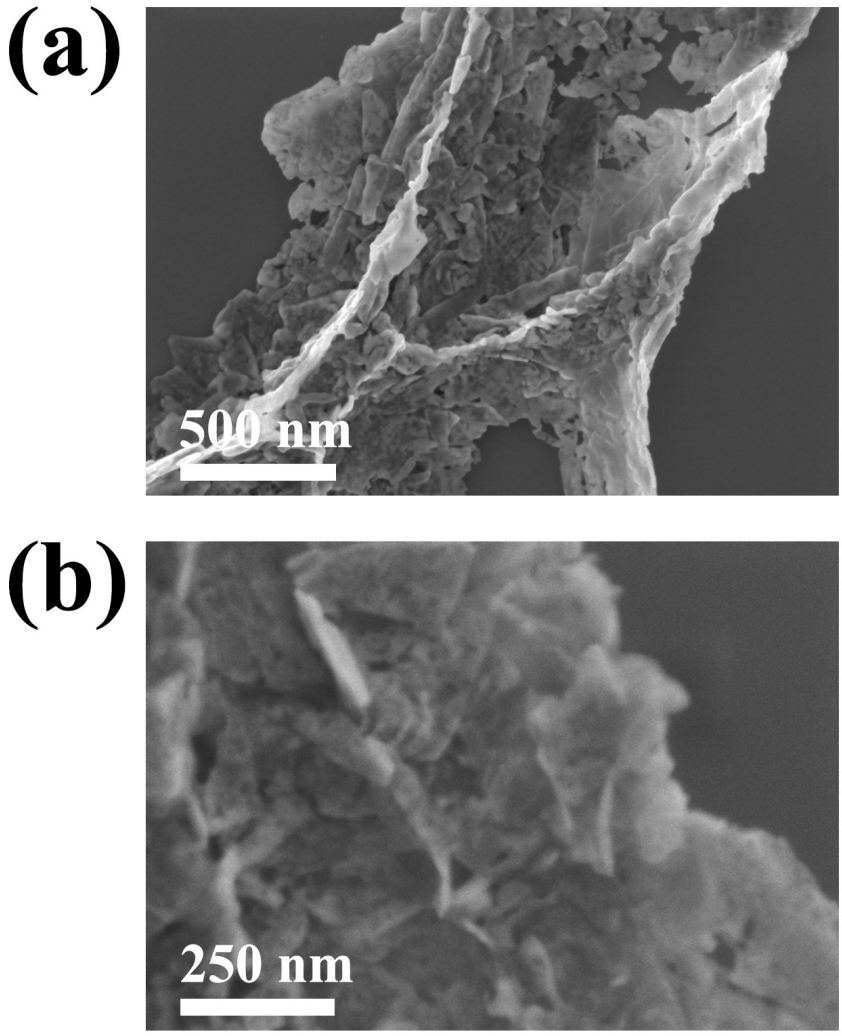

Fig. S4. SEM images of (a) $CuInP_2N_x$-400 and (b) $CuInP_2N_x$-500.

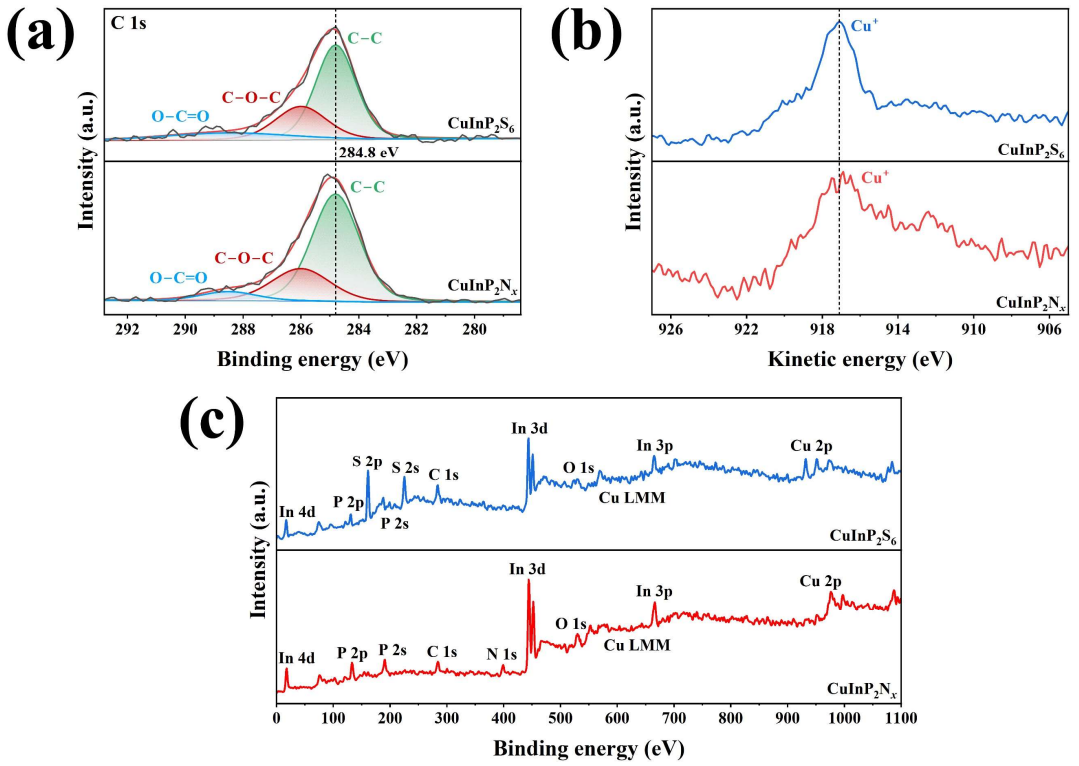

Fig. S5. (a) C 1s, (b) Cu LMM XPS spectra and (c) Survey of $CuInP_2S_6$ and $CuInP_2N_x$-300.

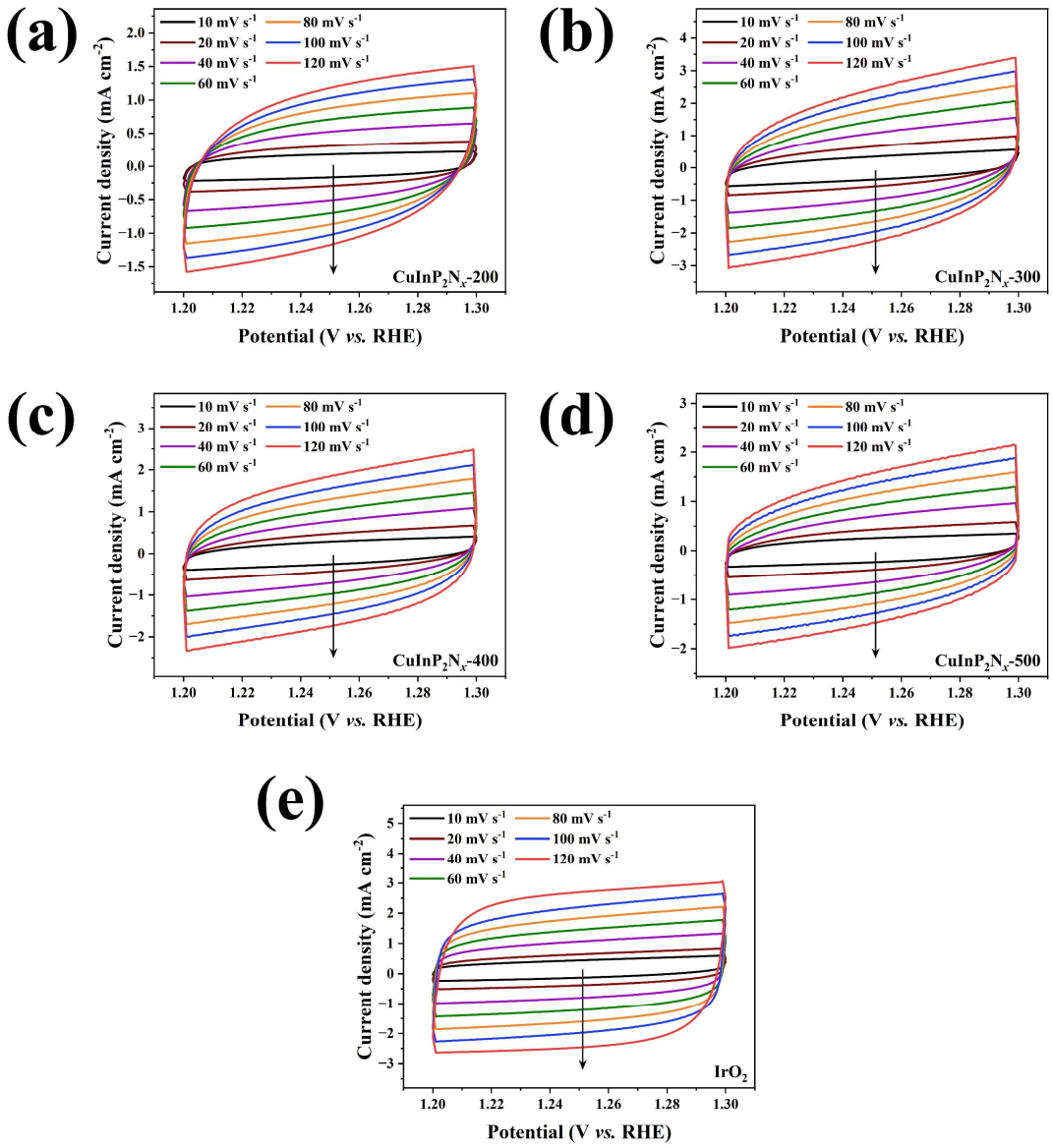

Fig. S6. Cyclic voltammetry (CV) curves of (a) $CuInP_2N_x$-200, (b) $CuInP_2N_x$-300 (c) $CuInP_2N_x$-400 (d) $CuInP_2N_x$-500 and (e) IrO_2 at different scan rates.

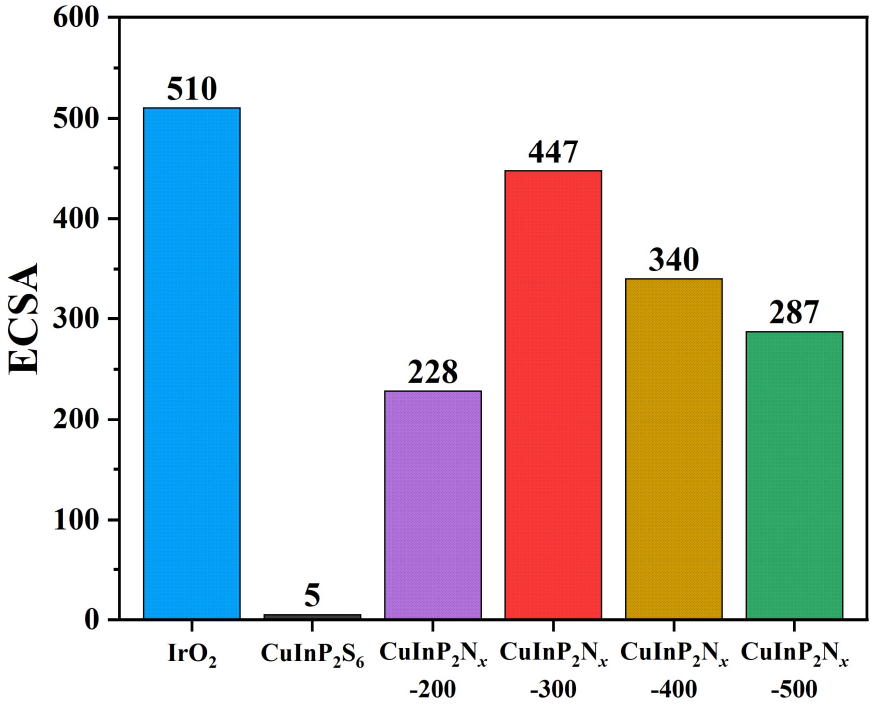

Fig. S7. Electrochemically active surface area (ECSA) of samples.

Calculation of ECSA is based on C_{dl} and C_s as follows:

$$ECSA_{(IrO_2)} = 20.4 \text{ mF cm}^2 \text{ / } 40 \text{ μF cm}^2 \approx 510$$

$$ECSA_{(CuInP_2S_6)} = 0.2 \text{ mF cm}^2 \text{ / } 40 \text{ μF cm}^2 \approx 5$$

$$ECSA_{(CuInP_2N_x\text{-}200)} = 9.1 \text{ mF cm}^2 \text{ /40 μF cm}^2 \approx 228$$

$$ECSA_{(CuInP_2N_x\text{-}300)} = 17.9 \text{ mF cm}^2 \text{ /40 μF cm}^2 \approx 447$$

$$ECSA_{(CuInP_2N_x\text{-}400)} = 13.6 \text{ mF cm}^2 \text{ / 40 μF cm}^2 \approx 340$$

$$ECSA_{(CuInP_2N_x\text{-}500)} = 11.5 \text{ mF cm}^2 \text{ / 40 μF cm}^2 \approx 287$$

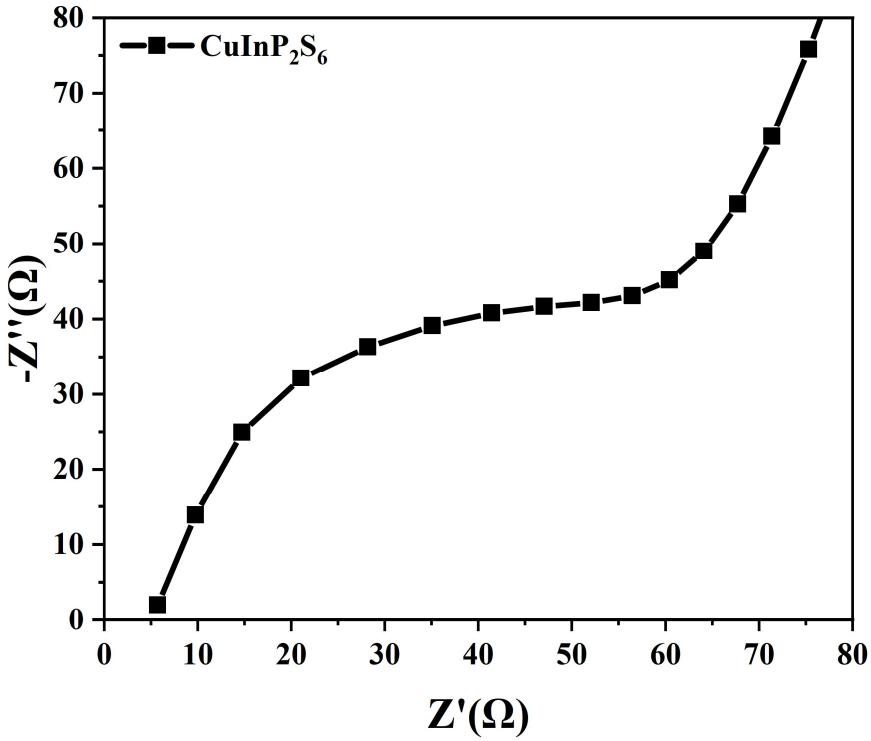

Fig. S8. Electrochemical impedance spectroscopy (EIS) of $CuInP_2S_6$.

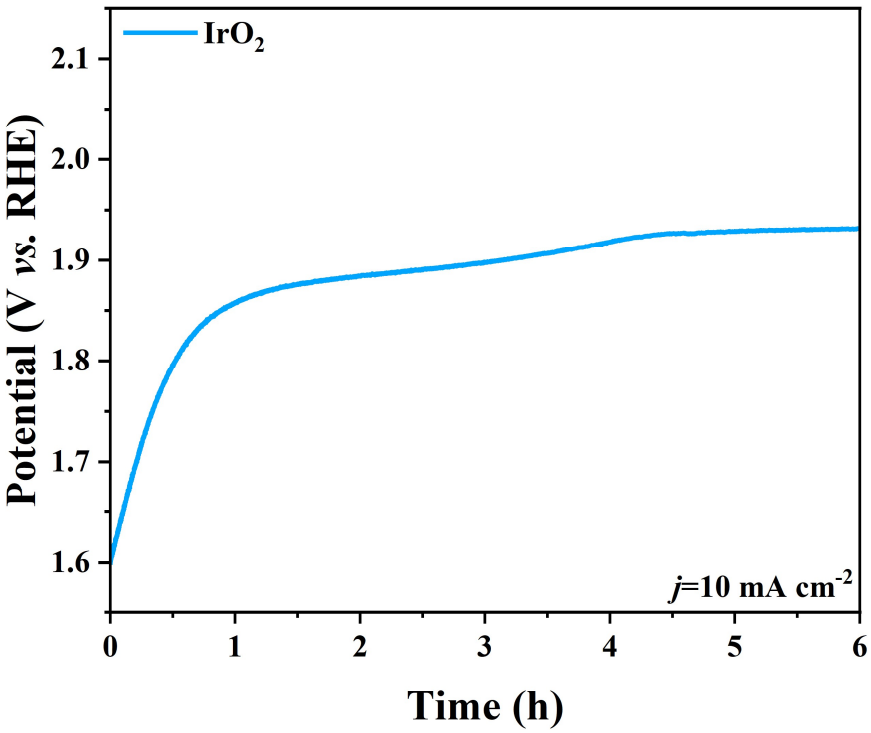

Fig. S9. Long-term stability test of IrO_2.

7.Tables

Table. S1. XPS quantitative analysis of $CuInP_2S_6$.

Element	Line Type	K-factor	Weight%	Atomic%
Cu	K	1.289	12.40	8.26
In	L	1.878	25.88	9.54
P	K	1.043	15.54	21.24
S	K	0.991	46.18	60.96
Total			100	100

Table. S2. XPS quantitative analysis of $CuInP_2N_x$-200.

Element	Line Type	K-factor	Weight%	Atomic%
Cu	K	1.289	20.12	13.96
In	L	1.878	40.60	15.59
P	K	1.043	21.66	30.83
N	K	3.481	8.68	27.33
S	K	0.991	8.94	12.29
Total			100	100

Table. S3. XPS quantitative analysis of $CuInP_2N_x$-300.

Element	Line Type	K-factor	Weight%	Atomic%
Cu	K	1.289	20.02	12.86
In	L	1.878	44.02	15.65
P	K	1.043	18.17	23.95
N	K	3.481	15.18	44.23
S	K	0.991	2.61	3.31
Total			100	100

Table. S4. XPS quantitative analysis of $CuInP_2N_x$-400.

Element	Line Type	K-factor	Weight%	Atomic%
Cu	K	1.289	20.27	12.57
In	L	1.878	41.95	14.40
P	K	1.043	19.20	24.43
N	K	3.481	16.26	45.74
S	K	0.991	2.32	2.86
Total			100	100

Table. S5. XPS quantitative analysis of $CuInP_2N_x$-500.

Element	Line Type	K-factor	Weight%	Atomic%
Cu	K	1.289	21.38	13.01
In	L	1.878	38.31	12.90
P	K	1.043	21.98	27.43
N	K	3.481	15.80	43.61
S	K	0.991	2.53	3.05
Total			100	100

Table. S6. Comparison of acidic OER performance.

Catalyst	Electrolyte	Overpotential (mV, 10 mA cm^{-2})	Tafel Slope (mV dec^{-1})	Stability	Ref.
CoSAs-MoS_2/TiN NRs	0.5 M H_2SO_4	454.9	165.5	45 h at 50 mA cm^{-2}	12
Co_2TiO_4	0.5 M H_2SO_4	513	320	10 h at 1.79V vs. RHE	13
N-doped graphite/carbon black	0.5 M H_2SO_4	470	226	-	14
RuIr nanocrystals	0.1 M $HClO_4$	344	111.5	5 h at 10 mA cm^{-2}	15
C_{60}–SWCNTs	0.5 M H_2SO_4	400	46.7	5 h at 1.7 V *vs.* RHE	16
2D Co_3O_4-250	0.5 M H_2SO_4	390	196	5 h at 10 mA cm^{-2}	17
40-IG	0.5 M H_2SO_4	276	57	4 h at 20 mA cm^{-2}	18
$CuInP_2N_x$-300	0.5 M H_2SO_4	356	159	60 h at 10 mA cm^{-2}	This work

Table. S7. Summary of R_s and R_{ct} in EIS measurement.

Sample	R_s	R_{ct}
IrO_2	6.9	31.1
$CuInP_2S_6$	4.4	63.6
$CuInP_2N_x$-300	5.6	33.8

8.References

1. S. Anantharaj, P. J. J. Sagayaraj, M. S. Yesupatham, R. Arulraj, K. Eswaran, K. Sekar and S. Noda, *J. Mater. Chem. A*, 2023, **11**, 17699-17709.
2. G. Kresse and J. Furthmüller, *Comput. Mater. Sci.*, 1996, **6**, 15-50.
3. G. Kresse and J. Furthmüller, *Phys. Rev. B*, 1996, **54**, 11169-11186.
4. P. E. Blöchl, *Phys. Rev. B*, 1994, **50**, 17953-17979.
5. J. P. Perdew, K. Burke, and M. Ernzerhof, *Phys. Rev. Lett.*, 1996, **77**, 3865-3868.
6. S. Grimme, J. Antony, S. Ehrlich and H. Krieg, *J. Chem. Phys.*, 2010, **132**, 154104.
7. J. Heyd, G. E. Scuseria and M. Ernzerhof, *J. Chem. Phys.*, 2003, **118**, 8207-8215.
8. J. Heyd, G. E. Scuseria and M. Ernzerhof, *J. Chem. Phys.*, 2006, **124**, 219906.
9. J. Rossmeisl, Z. W. Qu, H. Zhu, G. J. Kroes and J. K. Nørskov, *J. Electroanal. Chem.*, 2007, **607**, 83-89.
10. Á. Valdés, Z.-W. Qu, G.-J. Kroes, J. Rossmeisl and J. K. Nørskov, *J. Phys. Chem. C*, 2008, **112**, 9872-9879.
11. X.-C. Meng, J. Luan, Y. Liu, Y.-S. Sheng, F.-Y. Guo, P. Zheng, W.-L. Duan and W.-Z. Li, *J. Mater. Chem. A*, 2025, **13**, 627-637.
12. T. L. L. Doan, D. C. Nguyen, S. Prabhakaran, D. H. Kim, D. T. Tran, N. H. Kim and J. H. Lee, *Adv. Funct. Mater.*, 2021, **31**, 2100233.
13. S. Anantharaj, K. Karthick and S. Kundu, *Inorg. Chem.*, 2019, **58**, 8570-8576.
14. Y. Zhu, T. Zhang and J. Y. Lee, *ChemElectroChem*, 2018, **5**, 583-588.
15. J. Shan, T. Ling, K. Davey, Y. Zheng and S. Z. Qiao, *Adv. Mater.*, 2019, **31**, e1900510.
16. R. Gao, Q. Dai, F. Du, D. Yan and L. Dai, *J. Am. Chem. Soc.*, 2019, **141**, 11658-11666.
17. X. Yang, J. Cheng, H. Li, Y. Xu, W. Tu and J. Zhou, *Chem. Eng. J.*, 2023, **465**, 142745.
18. J. Chen, P. Cui, G. Zhao, K. Rui, M. Lao, Y. Chen, X. Zheng, Y. Jiang, H. Pan, S. X. Dou and W. Sun, *Angew. Chem. Int. Ed. Engl.*, 2019, **58**, 12540-12544.